Journal of Membrane Science & Research

journal homepage: www.msrjournal.com

Research Paper

Fabrication and Surface Characterization of Lignin-Polyamide Thin Film Composite Membrane for Reverse Osmosis Desalination

Mertella Lenie M. Ysulat [1, 2,*], Jan Anthony N. Ysulat [1], Alvin.R. Caparanga [2], Joseph.M. Pasag [1], Roland Andrew T. Cruz [1]

[1] *Industrial Technology Development Institute, DOST Compound, Gen. Santos Ave., Bicutan, Taguig City, Metro Manila, Philippines*
[2] *School of Chemical, Biological, and Materials Engineering and Sciences, Mapua University, Intramuros, Manila, Philippines*

Article info

Received 2023-03-21
Revised 2023-04-14
Accepted 2023-04-24
Available online 2023-04-24

Keywords

Lignin
Reverse osmosis
Thin film composite
Desalination
Membrane

Highlights

- Mechanically treated lignin nanoparticles (LNPs) were angular with low to medium sphericity
- The incorporation of LNPs in the polyamide layer altered the characteristics
- An increase in LNPs resulted in improved water flux and salt rejection
- Spray-based interfacial polymerization produced rougher surfaces than the conventional method

Graphical abstract

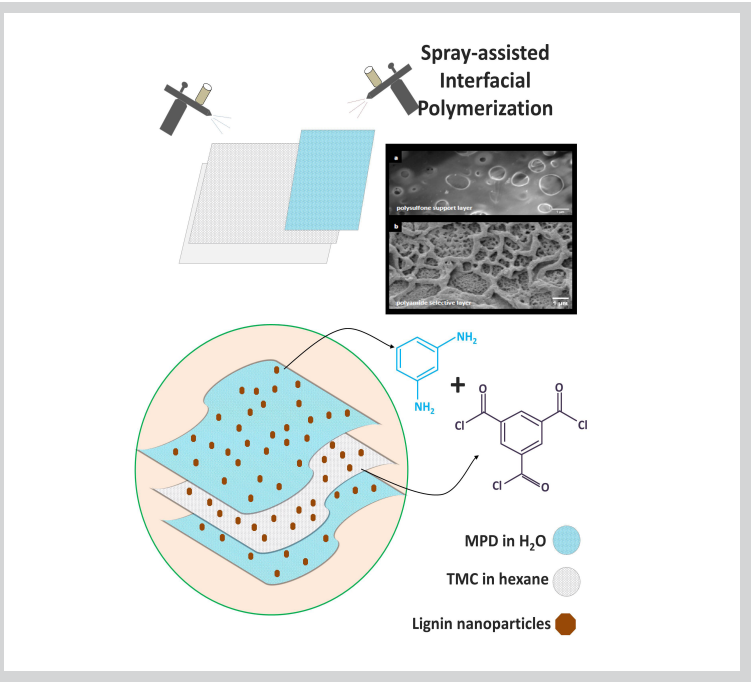

Abstract

Altering the intrinsic properties of thin film composites by integrating different nanoparticles has been widely explored in recent years. Sodium lignosulfonate (NaLS), lignin extracted by the sulfite process, was selected in this study because of its complex structure which contains both hydrophobic and hydrophilic moieties. NaLS was subjected to wet milling with n-hexane for 3 hours and 5 hours to reduce particle dimension to sub-micron size. The mechanical treatment has produced a mixture of spherical and angular/elongated particles with average size distributions of 408 nm for 3 hours of milling and 234 nm for 5 hours of milling. The polyamide selective layers with different concentrations of NaLS incorporated into the organic phase or aqueous phase were impregnated with the polysulfone support through conventional and spray-assisted interfacial polymerization (IP), respectively. The resulting composites fabricated through spray-based IP were observed to have rougher surfaces, Ra = 165 nm – 701 nm. Increased concentration of NaLS produced lower contact angles of 75.38° to 87.82° while the controls exhibited the highest readings ranging from 92.38° to 110.42°. Increased water flux and salt rejection were also observed for the modified PA-lignin TFC due to the enhanced hydrophilicity and a more negative surface charge.

1. Introduction

Reverse osmosis (RO), which accounts for 84% of the total desalination plants, produces 65.5 million cubic meters of desalinated water per day [1] by letting saline water flow through a series of semi-permeable membranes. The use of pressure, usually 50–80 bar for seawater, enables water molecules to enter the very minuscule pores of the membranes. Desalinated water is usually costlier than treated surface water or groundwater sources. This is due

* Corresponding author: mmysulat@itdi.dost.gov.ph (M. L. M. Ysulat)

DOI: 10.22079/JMSR.2023.1998807.1597

to the high energy requirement of the process and the sensitivity of the polymeric membranes which are prone to chemical, biological, and thermal degradation [2].

Scaling and fouling affect the overall performance and cost-effectiveness of the membrane. Several factors affect the susceptibility of a membrane to fouling, such as surface roughness and hydrophobicity. Hydrophobic membranes are more vulnerable to biofouling because they prefer to be coated with colloids rather than water. The polyamide-based active layer of thin film composite is hydrophobic in nature, thus, natural organic compounds can be easily adsorbed on its surface. The membranes need to be replaced eventually because regular cleaning cannot address the issue [3]. Higher surface roughness, on the other hand, permits microorganisms and ions to be trapped on the membrane's surface. It is therefore important to innovate novel membranes with new materials to produce robust RO performance with respect to water permeability, salt rejection, and resistance to fouling.

For the last few years, studies on the use of nanoparticles in membrane production are conducted to improve permeate quality, water flux, and fouling mitigation [4]. Membranes and composites with nanomaterials exhibit higher process efficiency and sorption rates compared to conventional membranes. Hemicellulose/cellulose, chitin/chitosan, glucans, protein, and linear polyesters were previously used in bio-nano composite synthesis [5]. Another bio-based polymer that is very abundant in nature but still underutilized is lignin.

Lignin, next to cellulose as the most abundant natural polymer, is typically found in cell walls of vascular plants and certain algae and constitutes approximately 20-35% [6] of plant biomass. Functionalities due to its complex structure present the feasibility of its use as phenolic or polyol feedstock for the synthesis of various polymers and composites. Commercially-available lignins are mainly byproducts of different pulping processes. The annual global production of lignin amounts to over 100 million tons, 70 million of which are produced by the pulping industry [7]. Approximately 95% are used for energy production by burning them in a recovery boiler. The remaining 5% is isolated from black liquor with acids such as H_2SO_4, H_3PO_4, or HCl or bases like NaOH and KOH and produce the technical lignins which are commercially available today as value-added products [8] such as dispersant, surfactant, and antioxidant in plastics and rubbers, and adhesive.

The most commercially traded technical lignin is sodium lignosulfonate (NaLS) which is a by-product of the sulfite pulping of wood. It is considered a surface-active agent or surfactant because it possesses both hydrophilic groups, such as sulfonate and carboxylic groups, and hydrophobic aliphatic and aromatic moieties. In previous works, surfactants were used to alter the surface properties of the polyamide (PA) layer of the thin film composites [9,10,11] and improve the overall efficiency of the RO membrane. Surfactants can also aid in interfacial polymerization (IP) by facilitating the transport of monomers to the organic phase from the aqueous phase [9].

This study, therefore, is focused on the surface modification of the polyamide selective layer of the thin film composite by the integration of sodium lignosulfonate (NaLS) nanoparticles into the aqueous phase or organic phase. Specifically, the research aimed to deliver the following objectives: to produce lignin nanoparticles by wet milling; to alter the surface characteristics of the PA selective layer by integrating lignin nanoparticles; and to characterize the lignin nanoparticles and lignin-PA TFC.

The results of this research will open new opportunities for lignin valorization while solving persisting challenges brought on by scaling and fouling on the RO TFC. Consequently, with the improved performance, the overall cost of operation and maintenance would be cut down. The preliminary findings provided insights on the potential effects of the acquired surface properties upon modification of the polyamide matrix, however, this study only covers the production and characterization of the lignin nanoparticles and lignin-reinforced composites while the optimization of the processes are beyond the scope of the research.

The novelty of this study is the incorporation of lignin nanoparticles onto the thin film composite's barrier layer by spray-assisted interfacial polymerization (IP) resulting in a multi-layered structure of lignin-polyamide matrices. This process could take advantage of NaLS' amphiphilic nature that could enhance the selective layer's surface properties, hence, improving the overall performance of the membrane.

2. Materials and Methods

2.1. Reagents used

Analytical grade of sodium lignosulfonate, together with the chemicals for the preparation of nanoparticles and thin film composites: n-hexane (>95%), N-methyl-2-pyrrolidone (NMP, 99%), Polysulfone (PSf, Mw = 35,000) pellets, m-Phenylenediamine (MPD, 99%), Triethylamine (TEA, 99%), trimesoyl chloride (TMC, 99%), and (1s)-(+)-10-camphorsulfonic acid (CSA, 99%), were purchased from different chemical suppliers and were used as is. All chemicals did not require pre-treatment or purification before use.

2.2 Production of Lignin Nanoparticles

LNPs were produced mechanically by wet milling. Thirty (30) grams of sodium lignosulfonate were soaked and dispersed in 100 ml n-hexane. Using 300g ZrO2 balls with a diameter of 1 mm, the suspension was subjected to fine grinding using a horizontal ball mill for 3-5 hours. Milled samples were collected upon decanting the n-hexane, air-dried until the excess solvent evaporated, and oven-dried at a temperature of 60°C for 30 minutes. Dried samples were stored in a tight container until use to prevent the absorption of water from the atmosphere.

2.3. Fabrication of Thin Film Composites

2.3.1. Polysulfone (PSf) Support Layer

To prepare the membrane support layer by the phase inversion method [12], PSf pellets were first dissolved in NMP solvent in a 15:85 (wt/wt) ratio. The mixture was homogenized by constant stirring using a hotplate stirrer for 6 hours at a temperature of 60°C. The clear solution was set aside overnight to allow degassing. The solution was poured over a backing paper, spread out on a glass plate, and cast to 130 μm using a four-sided film applicator. The sheet was submerged underwater to initiate the formation of the microporous PSf sublayer. The sheet was collected and stored in deionized water for 24 hours.

2.3.2. Polyamide-LNP Selective Layer

The thin selective layer was integrated into the PSf support layer through spray-based and conventional interfacial polymerization, depending on the phase where the LNPs were added. The optimized conditions for MPD and TMC contact times and curing temperature were obtained from a study conducted by Kadhom et. al. (2018) [13].

2.3.2.1. LNPs in Aqueous Phase – Spray-assisted IP

The LNPs were added to the MPD solution, containing 1% CSA/TEA and 2% MPD, with concentrations of 0.25% and 0.50% by weight. Using a pressurized portable airbrush with a nozzle opening of 0.3 mm, the aqueous phase was applied first to the PSf support sheet horizontally at a pressure of 2 bar. After 25 seconds, the TMC solution (0.15% in hexane) was sprayed over the MPD solution-covered substrate. The desired contact time for TMC was 5 seconds. This corresponds to one layer of polyamide matrix. Upon achieving the desired number of layers, 3 layers and 5 layers, the TFC membranes were dried at 80°C for 6 minutes. The micro-phase diffusion-controlled strategy was documented in the literature by Shan et. al. in 2017 [14].

2.3.2.2. LNPs in Organic Phase – Conventional IP

Milled lignin was added to the TMC solution (0.15% in hexane) at concentrations of 0.25% and 0.50%. The mixture was homogenized using a vortex mixer for 15 seconds. The polysulfone support sheet was first placed on flat glass. Excess water was absorbed by a squeegee roller then the sheet was immersed in MPD solution for 20 seconds and left to dry for 3.5 minutes at ambient temperature before immersing in TMC solution for 15 seconds. The sheet was dried in the oven for 6 min at a temperature of 80°C and was stored in DI water until use [13].

Fig. 1 demonstrates the different steps in fabrication of the thin film composite membrane.

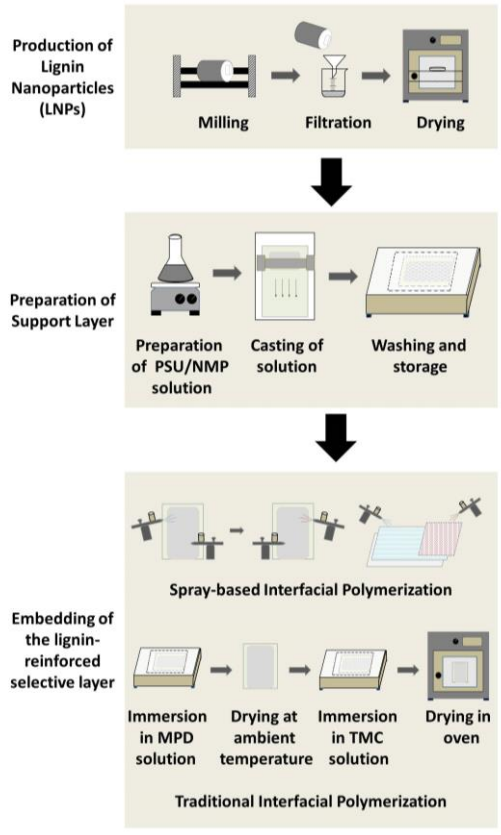

Fig. 1. Fabrication of thin film composite

2.4. Characterization of materials

2.4.1 Particle distribution of LNPs

The particle size distribution was determined through the Dynamic Light Scattering (DLS) method using Horiba Scientific nanoparticle SZ-100V2. Before the test, the powder samples were suitably dispersed in ethanol with the aid of an ultrasonic bath for 5 minutes.

2.4.2 Surface Morphology

The surface morphology of the Na lignosulfonate powders and thin film composites was examined with a Focused Ion Beam – Field Emission Scanning Electron Microscope (FIB-FESEM), FEI Helios Nanolab 600i Dual Beam System. Before imaging, a thin coating of platinum was embedded on the surfaces of the samples. The imaging was done using a secondary electron detector, Everhart Thornley Detector (ETD), in conjunction with the electron beam column operated at 2-kV accelerating voltage, 86-pA beam current, and 4-mm working distance. The SEM micrographs were examined using an open-source image processing program, ImageJ, to describe particle shapes qualitatively. On the other hand, the surface roughness of the thin-film composites was measured using an Atomic Force Microscope (AFM), Park Systems XE-100.

2.4.3 Membrane Wettability

The contact angle can indirectly determine the membrane's hydrophobicity or hydrophilicity which consequently affects its wetting ability. With the use of an optical tensiometer, Biolin Scientific Attention Theta Lite, the contact angles of the composites were measured through the sessile drop method at room temperature. The test started with gradually dropping 5 μL of distilled water over the membrane using a micro syringe. The equipment comes with a high-resolution camera and LED light to capture a very good image quality of the droplet. The contact angles were automatically measured by the software with fitting algorithms.

2.4.4. Performance Evaluation

The water flux and salt rejection of the RO membranes were tested using a fabricated cross-flow flat membrane filtration setup (Fig. 2). Each circular membrane was cut to an effective area of 12.56 cm^2 and was placed in a custom-made polymethyl methacrylate (PMMA) membrane cell. The unit was composed of 80-mm round PMMA discs with thicknesses of 19 mm and 10mm, a stainless steel sintered disc, and several 3-mm thick rubber gaskets, all screwed together to seal the system.

The membrane was first compacted at 0.6 MPa for 30 minutes with distilled water to condition the filter and stabilize the flux. The actual filtration process started with the 2000 ppm NaCl solution being pumped from a 3-L reservoir to the membrane cell by a diaphragm pump. The feed and retentate pressures were controlled to maintain a transmembrane pressure of 0.6 MPa at room temperature. The retentate was returned to the feed tank whereas the permeate was collected in a separate container.

After 20 minutes, water flux, J, in L/m^2-hr was determined by measuring the volume of permeated water:

$$J = \frac{V}{A \times t} \tag{1}$$

where V = permeate volume, A = membrane area, and t = accumulation time. Meanwhile, the salt rejection was estimated by the equation:

$$R\,[\%] = (1 - \frac{C_p}{C_f}) \times 100 \tag{2}$$

where, R is salt rejection, C_p is the permeate conductivity, and C_f is the feed conductivity [13].

The conductivities before and after filtration were measured using a pen-type conductivity meter (ES-1, China).

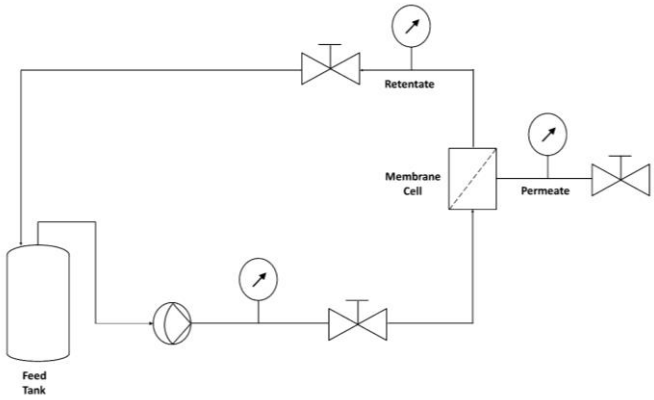

Fig. 2. Schematic diagram of the cross-flow filtration set-up

3. Results and Discussion

3.1. Production of Lignin Nanoparticles (LNPs)

Visually, the LNPs were lighter in color than the original sample. This can be explained by the mechanism by which the particles reflect light. Reflection of light can be classified into two types – specular reflection and diffuse reflection. The former occurs on smooth surfaces at a fixed angle while the latter is produced on rough surfaces wherein light is reflected at different angles and directions [15]. It is due to the diffuse reflection that the amount of the reflected milled samples [16]. This simple yet noticeable change in appearance gave a hint to the surface morphology of the LNPs.

It was also observed that after a few minutes of exposure to air, the LNPs started to dampen and eventually dissolved in the absorbed moisture from the atmosphere. This phenomenon is called deliquescence. By reducing the particle size, a larger surface area is exposed to air and as such, the dissolution becomes faster than normal. It is important to note that in the processing of hygroscopic materials such as NaLS, the relative humidity of the room should be constantly monitored and controlled.

3.2. Preparation of Thin Film Composite

The spray-assisted IP utilized in this study was inspired by the previous work of Shan et. al. in 2017 [14] where poly(ethyleneimine) (PEI) and trimesoyl chloride (TMC) were subjected to a micro-phase diffusion-controlled interfacial polymerization (MDC-IP) in which the bulk diffusion that is commonly observed in conventional IP was replaced by several micro-phase interfaces by applying the solutions by layers.

The surfaces of the fabricated thin film composites were smooth to the touch and did not bear any visual defect. The colors of the films produced by spray-based IP varied as the concentration of LNPs dissolved in the aqueous phase increased. A higher dosage of LNPs in the solution resulted in darker

surface color. Meanwhile, for the trials with LNPs dispersed in the TMC solution and applied by the conventional IP, the deposition of lignin can be observed as random brown dots on the surfaces of the skin layers. Interestingly, the LNPs seemed to have reacted to the aqueous phase upon contact causing these spots of varied sizes to appear.

3.3. Characterization of lignin nanoparticles

3.3.1. Chemical Structure

The IR spectra of the control and milled samples are shown in Fig. 3, and their peak assignments are listed in Table 1. The spectra show an observable broad band between 3200 cm^{-1} to 3500 cm^{-1}, indicating the stretching vibrations of hydroxyl groups (–OH) associated with phenols and alcohols. The characteristic peaks of lignin at 1569 cm^{-1} and 1408 cm^{-1} denote the C=C stretching of its aromatic ring. Symmetric SO_2=C=S is represented by the band at 1115 cm^{-1} [17] while S=O symmetric stretching vibrations of the –SO_3 groups are given by the weak peak at 1043 cm^{-1} [18]. The readings at 621 cm^{-1} [19], 648 cm^{-1}, and 925 cm^{-1} [20] reflect stretching vibrations of S–O of sulfonic groups. The latter also implies bending vibrations of OH bonds of carboxylic acids. The results of the ATR-FTIR confirm that there is no significant change in the chemical composition of the sodium lignosulfonate after milling for 3 hours and 5 hours.

Table 1
Peaks of NaLS and their corresponding assignments.

Wavenumber, cm^{-1}	Assignment
3200 -3500	ν of O-H
1569, 1408	C=C stretching
1043	νs(S=O) of –SO3
1115	symmetric SO2=C=S
925	ν(S–O) (R–SO3H), δ of OH bonds (R–COOH)
648, 621	*ν*(S–O) in R–SO3H

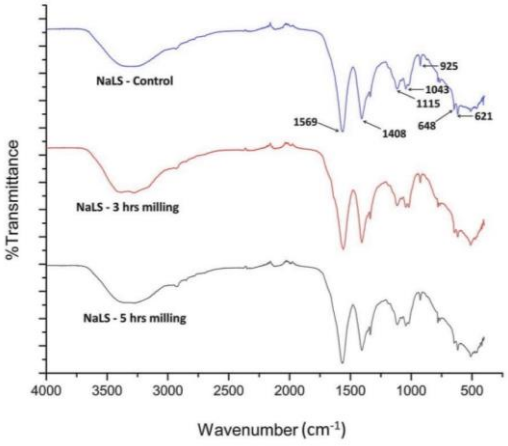

Fig. 3. IR spectra of Na-Lignosulfonates milled in 0, 3, and 5 hours.

3.3.2. Surface Morphology

Representative SEM micrographs of sodium lignosulfonates (NaLS) milled for 0, 3, and 5 hours are presented in Fig. 4. The images show that the lignin particles were initially slightly porous and spheroid in shape. After mechanical treatment, some particles became angular with low to medium sphericity. The measurements obtained using the ImageJ software reveal that almost 50% of the representative particles of milled samples were elongated and irregular in shape (circularity < 0.60). This explains also the change in color of the LNPs after hours of grinding as discussed in section 3.1. The reflectance was intensified because the rougher and angular surfaces of the particles enable the light to be diffused in different angles and directions.

The abundance of aggregates was also evident in the control and milled samples. Rezanowich [21] suggested that this self-association was caused by the interactions of hydrophobic moieties of the LNP while Li et. al. [22] proposed that the aggregates can form through the intramolecular hydrogen bonds in the absence of water. The aggregates, therefore, may start to form after drying the milled samples or during storage where LNPs have no contact with water molecules. The hydrogen bonds between the carboxyl, hydroxyl, and ether groups within the particle lead to intramolecular aggregation.

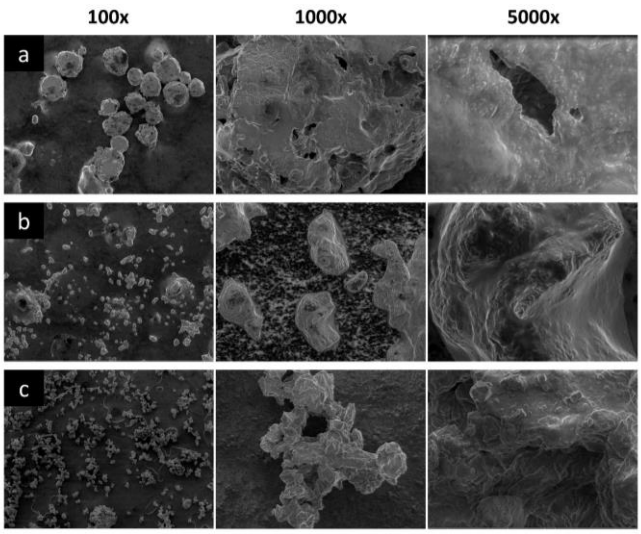

Fig. 4. SEM images of NaLS (a) Control, (b) 3 hrs milling, and (c) 5 hrs milling.

3.3.3. Particle size distribution

The particle size distributions of the NaLS samples determined by dynamic light scattering presented in Table 2 are averages of three readings per sample. It can be deduced from Fig. 5a, having two peaks, that there is a presence of bigger particles and aggregates in the untreated sample. Evidently, as the time of milling increases, the particle size becomes smaller. From 1 μm before the mechanical treatment, the size distribution narrows, having 50% of the particles downsized to 408 nm and 234 nm after 3 hours and 5 hours, respectively. Hence, the LNPs produced after 5 hours of milling were selected to be incorporated into the thin film composites.

Table 2
Particle size distribution of NaLS before and after milling.

	Particle Size, d(50), Average	
Control	3 hours milling	5 hours milling
1,094 nm	408 nm	234 nm

Visual inspection of SEM micrographs also gives us an insight that the powders have broad size distribution ranging from nano-sized to big micron-sized particles.

3.4. Characterization of lignin-reinforced thin film composites

3.4.1. Chemical Structure

The IR spectra recorded for the polyamide/polysulfone thin film composite are given in Fig. 6 while the peaks and their corresponding assignments are presented in Table 3. Characteristic peaks of polysulfone are recorded at 1244 cm^{-1} for C-O-C stretching and 1151 cm^{-1} for the O-S-O stretching. The strong transmittance reading at 1588 cm^{-1} is assigned to the bending vibration of N–H (amide II) while the C-N stretching of the amide can be observed at 1015 cm^{-1}. These peaks imply the successful formation of the polyamide layer over the polysulfone support.

Generally, the peaks of the lignin-deposited composites were the same as that of the control except for the weak peak at 1743 cm^{-1} corresponding to C=O stretching of ester compound brought about by the reaction of the carboxylic acid groups and the alcohols/phenols present in sodium lignosulfonate.

Table 3
Peaks of control and modified PA selective layer and their corresponding assignments.

Wave number	Assignment
1743	C=O stretching, ester, lactone
1588	N–H (amide II) vibration
1244	C-O-C stretching
1151	O-S-O stretching
1015	C-N stretching, amide

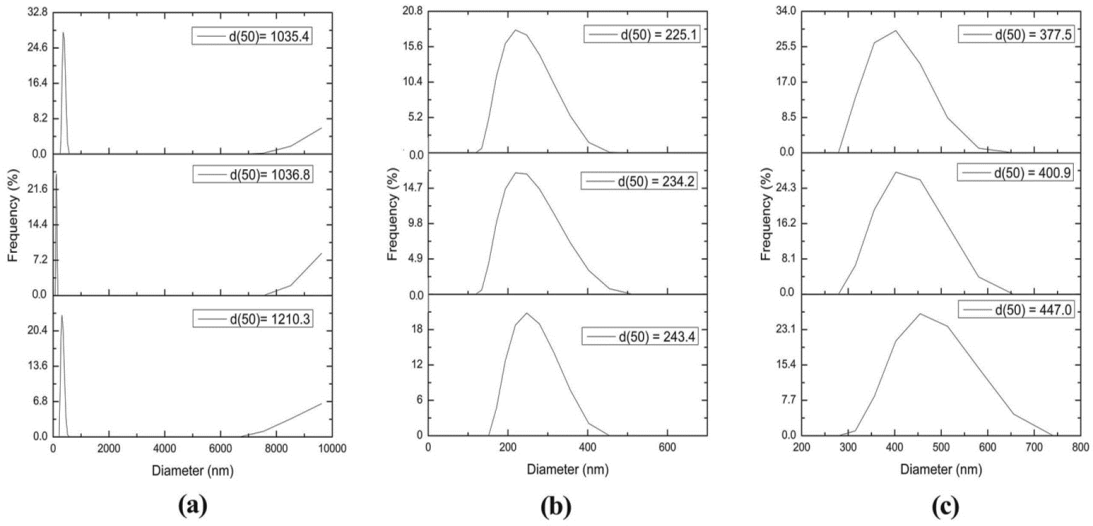

Fig. 5. Particle size distribution of (a) Control, (b) 3 hrs milling, and (c) 5 hrs milling

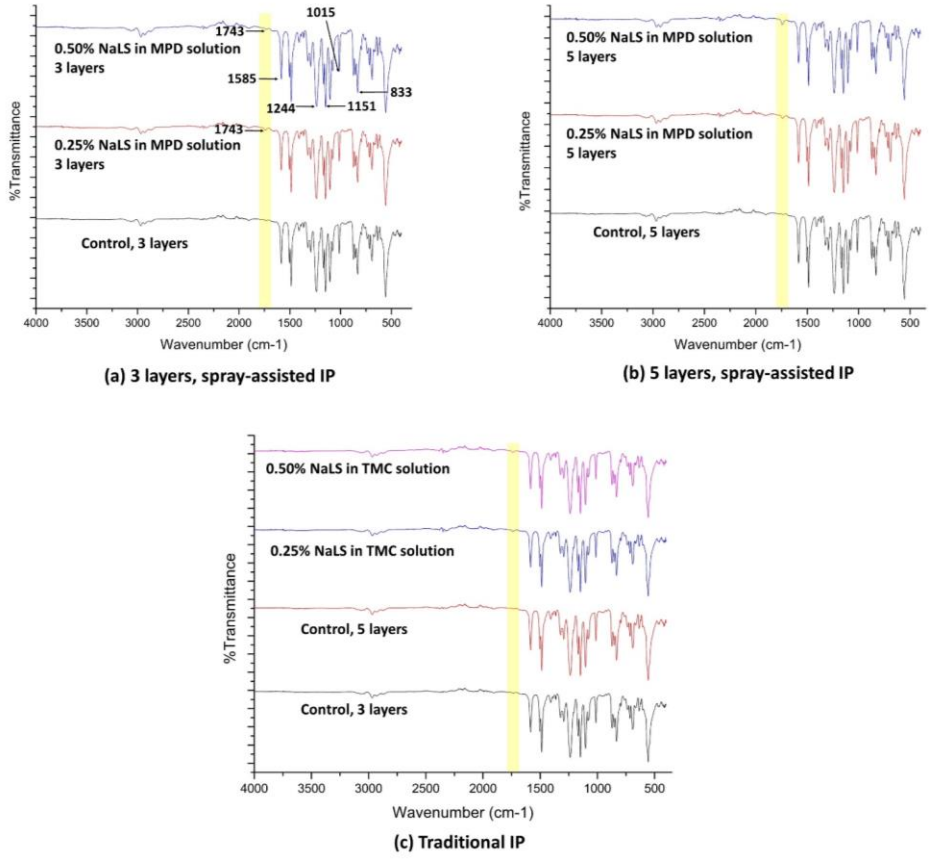

Fig. 6. IR spectra of the thin film composites fabricated by (a) 3 layers, spray-assisted IP, (b) 5 layers, spray-assisted IP, and (c) traditional IP

3.4.2. Surface Morphology

The SEM micrographs in Fig. 7 show the top surface of the fabricated thin film composites with a lignin-polyamide selective layer. The composites with sprayed selective layer exhibited "valley and ridge" texture on the surface which may be attributed to the internal structure of the polyamide matrix shown in Fig. 8. The interior shows a net-like arrangement with voids of different sizes. These voids were the result of the evaporation of hexane [14] during curing. The diameter and depth of each void depend on the size of the microdroplet of the aqueous MPD-lignosulfonate solution. Meanwhile, the surface of the trials with NaLS added to the TMC solution and deposited using the conventional interfacial polymerization was smoother given that the process applies a single layer of MPD-TMC assembly and does not require spraying or brushing of layers.

It was also observed that the surfaces of the films with LNPs looked brighter than the control samples. Due to electrostatic repulsion, secondary electron (SE), emission is assisted by the negative surface charges [23], [24]. The NaLS are sulfonated [25] and so they introduce negative charges to the surface of the selective layer. For this reason, the brightness of the images increased with higher LNP concentration. Spray-based assisted IP, where the LNPs are dissolved in the aqueous MPD solution, resulted in uniform brightness across the entire area whereas white patches seen in the surfaces of films produced by conventional IP are indicative of the embedded LNPs. The hydrophilic moieties of the LNPs reacted to an aqueous MPD solution giving the glow perceived at areas where the nanoparticles are situated.

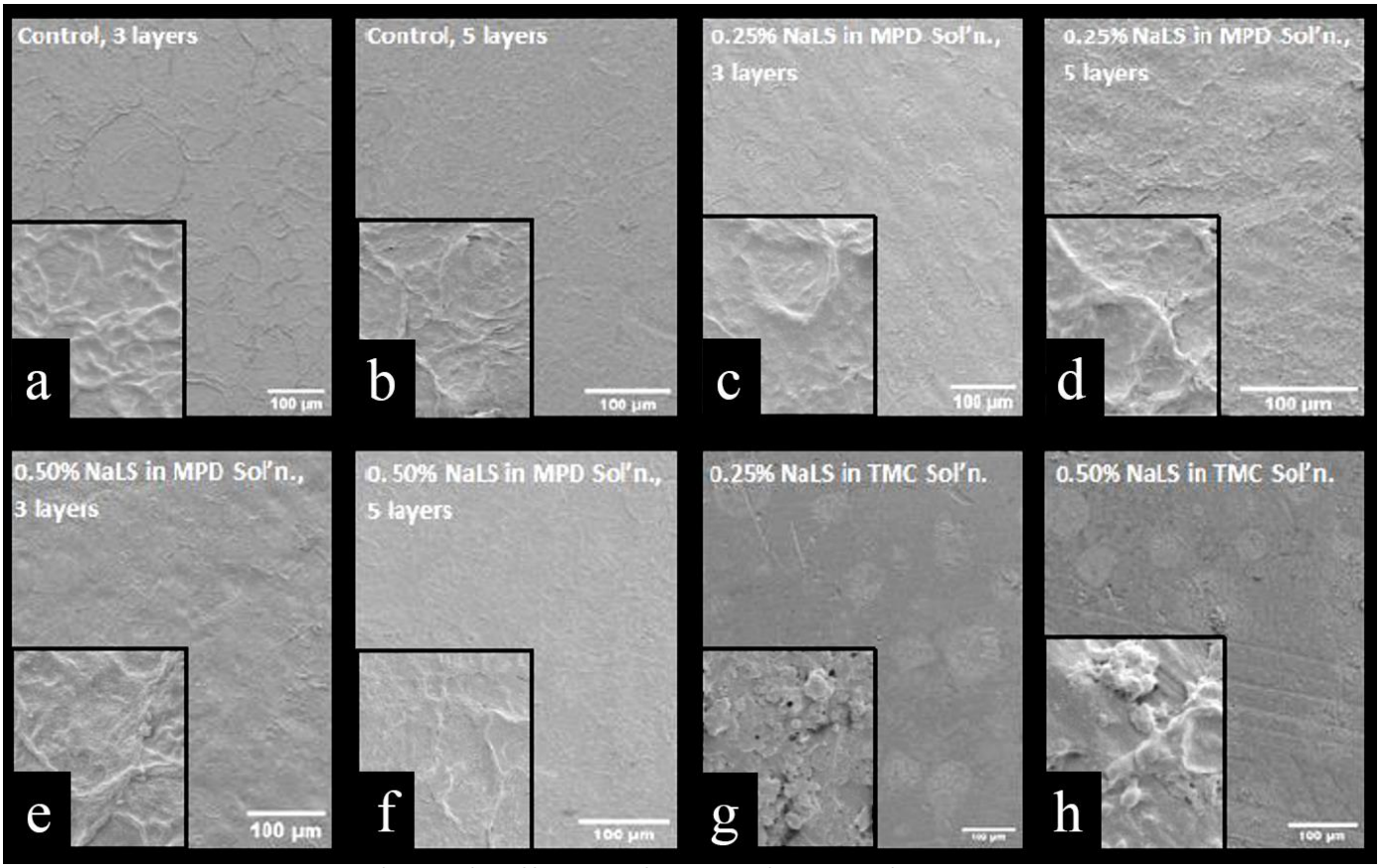

Fig. 7. SEM micrographs of the top surfaces of fabricated thin film composites fabricated by (a-f) spray-assisted IP and (g-h) traditional IP

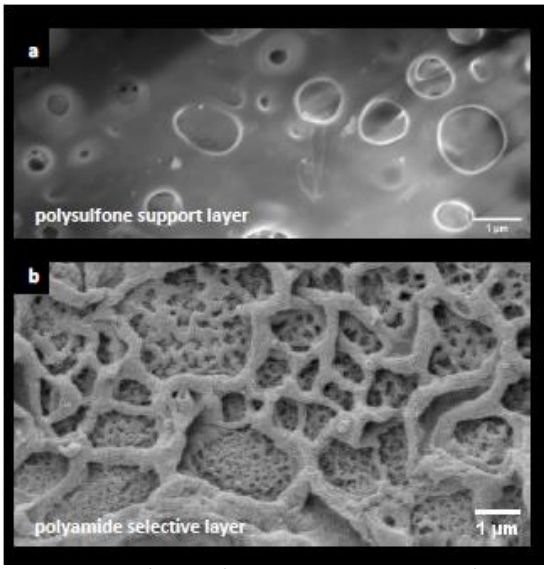

Fig. 8. Internal structures of the thin film composite layers (a) polysulfone support layer and (b) polyamide selective layer

The levels of texturization of the surfaces were estimated by the average surface roughness (Ra) calculated from AFM maps. The AFM images in Fig. 9 give us detailed landscapes of the barrier layer. The readings obtained coincide with the visual results of the SEM. Spray-based IP yielded rougher surfaces than the conventional IP, ranging from 165 nm – 701 nm, due to the depressions formed when the areas where droplets were sprayed dried up and the solvent evaporated during curing. It was observed from the images that the Ra generally increased with higher nanoparticle concentration. For spray-assisted IP, more areas were covered with thicker ridges of higher peaks likely due to the coalescence of neighboring droplets. The reduced interfacial tension of the aqueous droplets with the film caused by adding the surface active lignosulfonate facilitated the spreading of the liquid until colliding with the adjacent droplet and eventually merged to form larger ones [26].

3.4.3 Wettability

Membrane fouling is a persisting issue affecting the performance of membranes, specifically water flux and salt rejection. The features of the membrane's surface, such as porous structure, surface roughness, and hydrophobicity can impact the fouling potential of the membrane. Generally, more hydrophilic and smoother membrane surfaces are desired in addressing this challenge.

The control samples, both with 3 layers and 5 layers of the selective layer, have higher contact angle values, 92.38°, and 110.42°, respectively. Meanwhile, the readings of the samples with LNPs were lower ranging from 75.38° to 87.82° (Fig. 10).

The wetting of the composites' surfaces conforms to the Wenzel [27] model, Fig. 11, wherein the water droplet completely covers the rough surfaces of the membranes including their pores, thereby, providing a bigger liquid-solid contact surface area than smoother planes as displayed in Fig. 9. In this model, the apparent contact angle, θ_W, can be related to the intrinsic contact angle or the equilibrium contact angle when the droplet sits on a flat, smooth surface, θ:

$$\cos\theta_W = r\cos\theta \quad (3)$$

where r is the dimensionless parameter, roughness ratio, given by

$$r = \frac{actual\ total\ surface\ area}{projected\ area} \quad (4)$$

The value of r is always greater than 1, hence, for intrinsically hydrophilic surfaces whose θ<90°, θ_W becomes smaller and wetting is amplified. On the contrary, initially, hydrophobic surfaces become more hydrophobic in a Wenzel state of wetting.

Another explanation of the enhanced wettability of the modified membrane is the interaction of the carboxyl and sulfonic groups imparted by the LNPs embedded in the selective layer. These moieties form hydrogen bonds with the water molecules resulting in a decreased contact angle.

It is also worth noting that the contact angles of composites fabricated by spray-assisted IP gradually decreased over time as the liquid penetrated the cavities on the surface while in conventional IP, there is no significant change in the readings. However, the contact angles were still lower than that of the control samples due to the interaction of the lignin particles with the water.

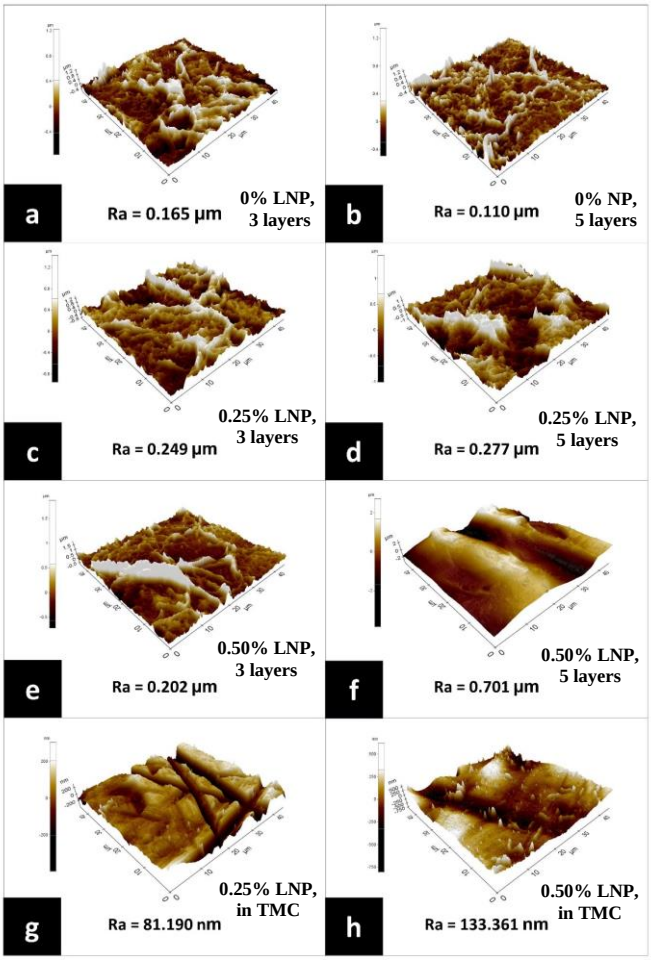

Fig. 9. AFM images of the composites fabricated by (a-f) spray-assisted IP and (g-h) traditional IP

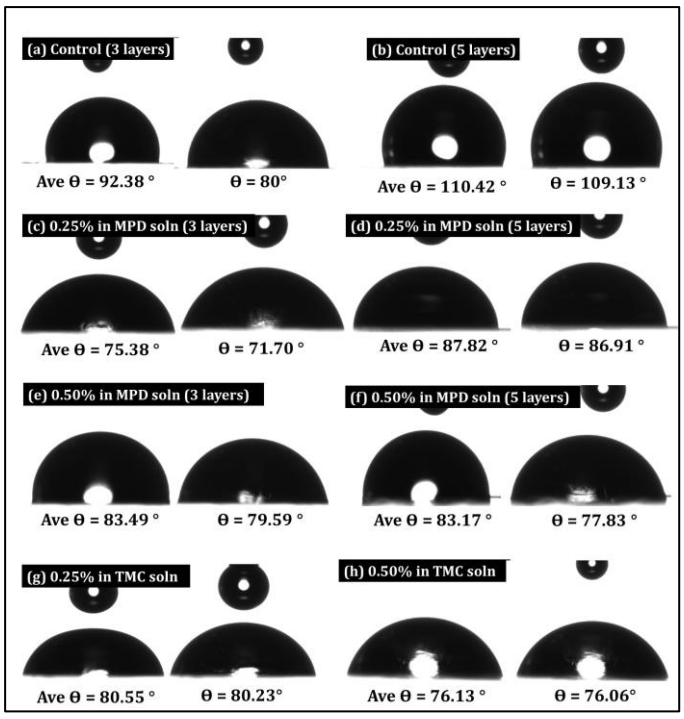

Fig. 10. Contact angle measurements of thin film composites with LNP

Fig. 11. Wettability of (a) smooth and (b) rough surfaces (Wenzel model)

3.4.4. Performance Evaluation

The water flux and salt rejection were presented in Fig. 12 for membranes with LNP incorporated in the MPD aqueous solution and in Fig. 13 for those that have the lignosulfonate added to the TMC solution, respectively. In all cases, the increase in lignosulfonate concentration, from 0 – 0.50% by weight, resulted in enhanced performance in terms of water flux and salt rejection.

The increase in water flux of the membranes with LNPs can be attributed to the negative charges imparted by the nanoparticles embedded in the selective layer coupled with increased hydrophilicity [28]. The modified surface of the polyamide barrier facilitates the transport of water through the membranes more efficiently. For membranes with 3 coats and 5 coats of PA-lignin layer, both having 0.50% LNP concentration in the MPD solution, recorded a water flux of 217.95 L/m^2-hr and 159.32 L/m^2-hr, respectively.

On the other hand, the Donnan electrostatic exclusion (DEE) principle explains the improved salt rejection of the modified membranes. The presence of more negatively charged moieties on the top surface of the PA-lignin layer caused the repulsion of the anions present in the feed while attracting the cations. This makes the concentration of the anion lesser on the surface of the membrane than in the bulk solution. Consequently, Donnan potential is induced at the interface between the membrane and the feed. The Donnan potentials of the modified membranes were negative and so anions were repelled more easily and cations were retained on the membrane's surface to maintain electroneutrality. Among all the trials, those that have their LNPs added in the organic phase at 0.25% and 0.50% by weight concentration recorded the highest salt rejection of 87.91% and 86.62%, respectively. This may be because the negatively charged functional groups of lignin were readily exposed as the TMC solution was always the last to be incorporated in the PA-lignin matrix.

Another possible reason for the higher salt rejection of LNP-enforced membranes is the dilution effect in which the concentration of the ions in the permeate decreases as water flux increases. Both trials with 0.50% LNPs in MPD solution exhibited the highest salt rejection in their respective groups given that they also had the highest results for water flux.

For comparison, Table 4 gives a summary of the performances of thin-film composites with lignin embedded in the selective layer by traditional IP or immersion in monomer solutions. The operating pressure of the cross-flow filtration, preferably close to 0.6 MPa which was used in this study, was considered in the selection of the composites for comparison. It can be seen that the performance of the produced lignin-modified membrane in terms of salt rejection was at par with that of the published works.

Improvement in the spray-assisted IP process can be explored by altering different parameters such as (1) different exposure times of the organic and aqueous phases and (2) the size of droplets of the monomer solution by varying the pressure of the air spray gun.

Moreover, optimization of the production of lignin nanoparticles by the mechanical process can be further explored. Preliminary results suggest that in preparation of lignin nanoparticles by wet milling, relative humidity (%RH) should be monitored and controlled to reduce the risk of aggregation and deliquescence. Increasing the milling time may be done, however, it is not financially practical because of the additional electricity requirement.

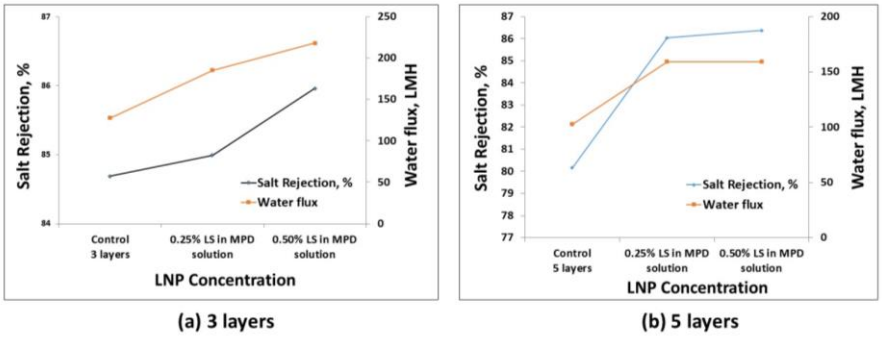

Fig. 12. Salt rejection and water flux of membranes fabricated by spray-assisted IP

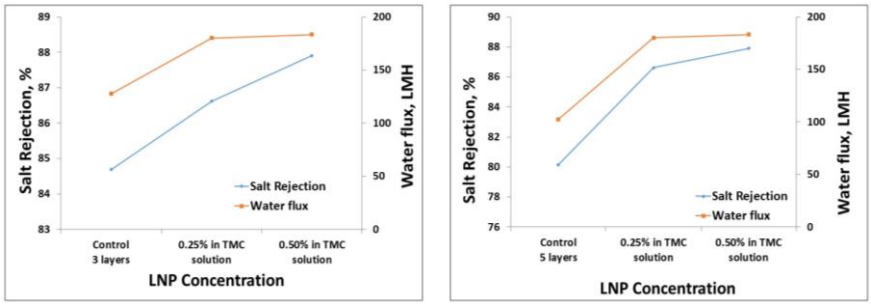

Fig. 13. Salt rejection and water flux of membranes fabricated by traditional IP

Table 4
Salt rejection of lignin-modified composites

Membrane Composition / Process	Salt Used	Operating Pressure	Salt Rejection	Reference
Lignin-PA-PSf				
a. 0.25% - 0.50% in aqueous MPD solution (Spray-based IP)			85 - 86%	
a.1. 3 layers				
a.2. 5 layers	2,000 ppm NaCl	0.6 MPa	86%	Current study
b. 0.50% in organic phase – TMC solution (Traditional IP)			87.91%	
Lignin/PEI-PSf	2,000 ppm $MgSO_4$		51.4%	
a. 0.20% PEI + 0.30% NaLS				
(Layer-by-layer deposition - immersion in electrolyte solutions)				
b. With glutaraldehyde (GA) as a crosslinker (1%, w/w)				
b.1. 30 mins crosslinking		1.0 MPa	77.8%	[29]
b.2. 60 mins crosslinking			90.3%	
c. With supporting electrolyte (NaCl)			91.7%	
c.1. 0.25M NaCl			<60%	
c.2. 1 M NaCl	2,000 ppm NaCl		37.9%	
Alkaline lignin (AL) /TMC-PSf				
2% AL solution+0.1% TMC solution				
(Traditional IP)				
a. Aminated AL	1,000 ppm NaCl	0.5 MPa	23.7%	[30]
	1,000 ppm $MgSO_4$		14.6%	
b. Pristine AL	1,000 ppm NaCl		~15%	
	1,000 ppm $MgSO_4$		~10%	
Lignin alkali (LA) /TMC-PSf	1 M $MgSO_4$	1 MPa	51.4%	[31]
2% w/w LA + 0.3% w/w TMC				
(Traditional IP)	1 M NaCl		31.8%	

4. Conclusion

Lignin nanoparticles (LNPs) were successfully produced by simple wet milling of sodium lignosulfonate with n-hexane. After mechanical treatment, the product was a combination of micron-sized and nano-sized spherical and angular/elongated particles with size distributions of 408 nm for 3 hours of milling and 234 nm for 5 hours of milling. The IR spectra recorded by ATR-FTIR confirmed that the chemical structure of the lignosulfonate was not altered.

Surface modification of the polyamide selective layer by the addition of the LNPs at concentrations of 0.25% and 0.50% by weight and the method of their deposition were studied. The weak peak at 1743 cm^{-1} of the material's IR spectra implies the occurrence of ester compounds formed during the incorporation of lignosulfonates in the polyamide matrix.

Spray-assisted interfacial polymerization produced a rougher texture with average surface roughness ranging from 165 nm – 701 nm. This is due to the depressions formed during the evaporation of n-hexane from the droplets. The depth and size of the voids are dependent on the volume and the surface covered by the droplets. Due to the reduced interfacial tension between the liquid and the surface upon the addition of LNPs, the droplets spread wide and merge with the neighboring droplets causing larger and deeper voids and thicker ridges. Meanwhile, the selective layer deposited by conventional IP exhibited a smoother surface. Higher concentrations of the LNPs in both methods gave higher Ra than the control samples.

The successful integration of the lignosulfonate particles into the selective layer was also validated by the SEM. The modified polyamide layers produced brighter images because of the negative charges imparted by the LNPs.

The contact angles of the modified composites were lower (θ = 75.38° - 87.82°) compared to the unmodified samples (θ = 92.38° - 110.42°). The integration of LNPs in either the aqueous phase or organic phase resulted in reduced interfacial tension between the surface and the water and increased surface roughness. Consequently, the water can easily spread across the surface and penetrate the voids, further enhancing the wettability of the surface.

The incorporation of lignin nanoparticles in the polyamide layer altered the characteristics of the surface concerning the roughness, wettability, and surface charge. These three properties considerably influenced the performance of the RO membrane, in terms of water flux and salt rejection. PA-lignin matrix exhibited higher water flux and salt rejection values ranging from 159 - 217 L/m^2-hr and 84.99% - 87.91%, respectively.

The initial results obtained may give a hint about the biofouling resistance of the fabricated membranes. A hydrophilic and negatively charged surface can inhibit biofouling. Through electrostatic repulsion, the adhesion and accumulation/growth of the negatively charged foulants, such as most microorganisms [32] to the surface of the membrane would be prevented [33,34], thus, maintaining the efficiency of the membrane's performance and prolonging its life.

In terms of surface roughness, rougher surfaces are more prone to fouling and scaling. The valley and ridges structure of the polyamide layer provides areas where foulants and ions are trapped and accumulated over time [32,33]. Eventually, the water permeability would decline if these problems are not addressed properly.

The continuation of this study is recommended to confirm the effects of surface modification on the performance of the polyamide selective layer. While initial results suggest that the modified membranes exhibited improved performance, it is still fitting to carry out additional tests by cross-flow filtration using varying transmembrane pressure, feed concentration, and pH. These factors are influential to the overall performance of the RO membranes.

Acknowledgment

The authors would like to acknowledge the support given by the Department of Science and Technology – Industrial Technology Development Institute (ITDI), specifically the Chemicals and Energy Division (CED), Materials Science Division (MSD), Standards and Testing Division (STD), Planning and Management Information Systems Division (PMISD), and the Advanced Device and Materials Testing Laboratory (ADMATEL). Appreciation is also given to Globesco Incorporated, Molan Plastic Technology Co. Ltd., and Shandong Gaotang Kelin Environmental Protection Technology Co. Ltd. for supplying some of the instruments and materials for the study.

Funding

This work was financially supported by the Department of Science and Technology – Science Education Institute under the Human Resource Development Program.

CRedit authorship contribution statement

M.L.M Ysulat: Data curation; Writing - original draft; Formal analysis; Funding acquisition; Investigation; Methodology.
J.A.N Ysulat: Investigation; Methodology.
A.R. Caparanga: Conceptualization; Supervision; Validation; Visualization.
J.M. Pasag: Conceptualization; Data curation.
R.A.T. Cruz: Conceptualization; Data curation.

Declaration of Competing Interest

The authors declare that they have no known competing financial interests or personal relationships that could have appeared to influence the work reported in this paper.

References

[1] E. Jones, M. Qadir, M. van Vliet, V. Smakhtin, S. M. Kang, The state of desalination and brine production: A global outlook. Sci. Total Environ. 657 (2019) 1343–1356. https://doi.org/10.1016/j.scitotenv.2018.12.076.

[2] L. Setiawan, R. Wang, A. G. Fane, Fabrication of novel poly(amide-imide) forward osmosis hollow fiber membranes with a positively charged nanofiltration-like selective layer. J. Membr. Sci. 369 (2015) 196-205. https://doi.org/10.1016/j.memsci.2010.11.067.

[3] V. Freger, J. Gilron, S. Belfer, TFC polyamide membranes modified by grafting of hydrophilic polymers: an FT-IR/AFM/TEM study. J. Membr. Sci. 209 (2002) 283–292. https://doi.org/10.1016/S0376-7388(02)00356-3.

[4] K. A. Mahmoud, B. Mansoor, A. Mansour, M. Khraisheh, Functional graphene nanosheets: the next generation membranes for water desalination. Desalination 356 (2015) 208–225. https://doi.org/10.1016/j.desal.2014.10.022.

[5] R. Dongre, K. Sadasivuni, K. Deshmukh, A. Mehta, S. Basu, J. Meshram, M. Al-Maadeed, A. Karim, Natural polymer-based composite membranes for water purification: a review. Polym.-Plast. Technol. Mater. 58 (2019) 1295-1310. https://doi.org/10.1080/25740881.2018.1563116.

[6] A. Naseer, A. Jamshaid, A. Hamid, N. Muhammad, M. Ghauri, J. Iqbal, S. Rafiq, S. Khuram, N. Shah, Lignin and Lignin Based Materials for the Removal of Heavy Metals from Waste Water-An Overview. Z. Phys. Chem. 233 (2018). https://doi.org/10.1515/zpch-2018-1209.

[7] H. Luo, M. M. Abu-Omar, Chemicals from lignin, in: M. A. Abraham, Encyclopedia Sustainable Technologies, Elsevier Inc., Massachusetts, 2017, pp. 573–585, https://doi.org/10.1016/b978-0-12-409548-9.10235-0.

[8] P. Schulze, M. Leschinsky, A. Seidel-Morgenstern, H. Lorenz, Continuous Separation of Lignin from Organosolv Pulping Liquors - Combined Lignin Particle Formation and Solvent Recovery. Ind. Eng. Chem. Res. 58 (2019). https://doi.org/10.1021/acs.iecr.8b04736.

[9] F. Azarteimour, M. Amirinejad, M. Parvini, S. S. Madaeni, Anionic/Non-ionic Surfactants in Aqueous Phase of Thin Film Composite Poly(Paraphenylene Terephthalamide) Nanofiltration Membranes. J. Membr. Sci. Res. 3 (2017) 13-21. https://doi.org/10.22079/jmsr.2017.23342.

[10] K. Baransi-Karkaby, M. Bass, S. Levchenko, S. Eitan, V. Freger, Facile Modification of Reverse Osmosis Membranes by Surfactant-Assisted Acrylate Grafting for Enhanced Selectivity. Environ. Sci. Technol. 51 (2017) 2347–2354. https://doi.org/10.1021/acs.est.6b05260.

[11] H. D. Raval, M. R. Raviya, H. C. Rathod, Polyamide-surfactant interaction: Exploration of new avenues for reverse osmosis separation applications. Adv. Polym. Technol. 37 (2018) 3106–3114. https://doi.org/10.1002/adv.22081.

[12] M. Kadhom, J. Yin, B. Deng, A Thin Film Nanocomposite Membrane with MCM-41 Silica Nanoparticles for Brackish Water Purification. Memb. 6 (2016) 50. https://doi.org/10.3390/membranes6040050.

[13] M. Kadhom, B. Deng, Synthesis of high-performance thin film composite (TFC) membranes by controlling the preparation conditions: Technical

notes. J. Water Process. Eng. 30 (2018). https://doi.org/10.1016/j.jwpe.2017.12.011.
[14] L. Shan, J. Gu, H. Fan, S. Ji, G. Zhang, Microphase Diffusion-Controlled Interfacial Polymerization for an Ultrahigh Permeability Nanofiltration Membrane. ACS Appl. Mater. Interfaces 9 (2017) 44820–44827. https://doi.org/10.1021/acsami.7b14017.
[15] A. K. R. Choudhury, Principles of Colour and Appearance Measurement, Woodhead Publishing, Masachussette, 2014. https://doi.org/10.1533/9780857099242.53
[16] M. G. Lagorio, Why Do Marbles Become Paler on Grinding? Reflectance, Spectroscopy, Color, and Particle Size. J. Chem. Educ. 81 (2004) 1607-1611. https://doi.org/10.1021/ed081p1607.
[17] T. Dasilva, R. W. Sudrajat, M. Kasmiyatun, S. Priyanto, B. Pramudono, A. Fauzan, Synthesis of Sodium Lignosulfonate (SLS) Surfactant and Polyethylene Glycol (PEG) as Surfactants in Enhanced Oil Recovery (EOR). IOP Conf. Ser. Mater. Sci. Eng. 1053 (2021) 012068. https://doi.org/10.1088/1757-899x/1053/1/012068.
[18] X. Ji, M. Guo, L. Zhu, W. Du, H. Wang, Synthesis Mechanism of an Environment-Friendly Sodium Lignosulfonate/Chitosan Medium-Density Fiberboard Adhesive and Response of Bonding Performance to Synthesis Mechanism. Mater. 13 (2020) 5697. https://doi.org/10.3390/ma13245697
[19] P. Rodríguez-Lucena, J. J. Lucena, L. Hernández-Apaolaza, Relationship between the structure of Fe-Lignosulfonate complexes determined by FTIR spectroscopy and their reduction by the leaf Fe reductase. UC Davis: Department of Plant Sciences (2009). Retrieved from https://escholarship.org/uc/item/9k69q71d
[20] I. A. Palamarchuk, O. S. Brovko, K. G. Bogolitsyn, T. A. Boitsova, A. V. Ladesov, A. D. Ivakhnov, Relationship of the structure and ion-exchange properties of polyelectrolyte complexes based on biopolymers. Russian J. Appl. Chem. 88 (2015) 103–109. https://doi.org/10.1134/s1070427215010152.
[21] A. Rezanowich, W. Q. Yean, D. A. I. Goring, High-resolution electron microscopy of sodium lignin sulfonate. J. Appl. Polym. Sci. 8 (1964) 1801–1812. https://doi.org/10.1002/app.1964.070080429.
[22] H. Li, Y. Deng, H. Ye, L. Xiao, X. Qiu, Effect of Temperature on Polyelectrolyte Expansion of Lignosulfonate. BioResour. 10 (2015) 575-587. https://doi.org/10.15376/biores.10.1.575-587.
[23] K. Suemori, Y. Watanabe, N. Fukuda, S. Uemura, Voltage Contrast in Scanning Electron Microscopy to Distinguish Conducting Ag Nanowire Networks from Nonconducting Ag Nanowire Networks. ACS Omega 5 (2020) 12692–12697. https://doi.org/10.1021/acsomega.9b04222.
[24] M. T. Postek, A. E. Vladár, Does Your SEM Really Tell the Truth?-How Would You Know? Part 4: Charging and its Mitigation. Proc. SPIE - Int. Soc. Opt. Eng. 9636 (2015) 963605. http://dx.doi.org/10.1117/12.2195344.
[25] T. Aro, P. Fatehi, Production and Application of Lignosulfonates and Sulfonated Lignin. ChemSusChem 10 (2017) 1861–1877. https://doi.org/10.1002/cssc.201700082.
[26] J. Jin, C. H. Ooi, D. V. Dao, N. T. Nguyen, Coalescence Processes of Droplets and Liquid Marbles. Micromachines, 8 (2017) 336. https://doi.org/10.3390/mi8110336.
[27] B. J. Ryan, K. M. Poduska, Roughness effects on contact angle measurements. Am. J. Phys. 76 (2008) 1074–1077. https://doi.org/10.1119/1.2952446.
[28] J. Wang, Z. Wang, J. Wang, S. Wang, Improving the water flux and bio-fouling resistance of reverse osmosis (RO) membrane through surface modification by zwitterionic polymer. J. Membr. Sci. 493 (2015) 188–199. http://dx.doi.org/10.1016/j.memsci.2015.06.036
[29] W. Liu, X. Geng, S. Li, X. Zhan, J. Li, L. Wang, J. Lei, Preparation of lignosulfonate-based nanofiltration membranes with improved water desalination performance. Eng. Life Sci. 21 (2021) 417–428. https://doi.org/10.1002/elsc.202000102.
[30] W. Sun, N. Zhang, Q. Li, X. Luo, H. Baqiah, W. Cui, Z. Li, H. Deng, Lignin-based Nanofiltration Membrane with High Permeability, Acid-alkali, and Chlorine Resistances toward the Removal of Multivalent Salts and Dyes. Chem. Lett. 51 (2022) 945–948. https://doi.org/10.1246/cl.220292.
[31] S. Zhan, S. Li, X. Zhan, J. Li, J. Lei, L. Wang, Green lignin-based polyester nanofiltration membranes with ethanol and chlorine resistance. J. Appl. Polym. Sci. 139 (2022) 51427. https://doi.org/10.1002/app.51427.
[32] H. Maddah, A. Chogle, Biofouling in reverse osmosis: phenomena, monitoring, controlling and remediation. Appl. Water Sci. 7 (2016) 2637–2651. https://doi.org/10.1007/s13201-016-0493-1.
[33] L. Xie, Y. Liu, W. Zhang, S. Xu, A Dopamine/Tannic-Acid-Based Co-Deposition Combined with Phytic Acid Modification to Enhance the Anti-Fouling Property of RO Membrane. Membranes, 11 (2021) 342. https://doi.org/10.3390/membranes11050342.
[34] J. Yang, S. Lee, E. Lee, J. Lee, S. Hong, Effect of solution chemistry on the surface property of reverse osmosis membranes under seawater conditions. Desalination 247 (2009) 148–161. https://doi.org/10.1016/j.desal.2008.12.020.